Cell

Sensitivity-Enhanced NMR Reveals Alterations in Protein Structure by Cellular Milieus

Graphical Abstract

Highlights

- Sensitivity-enhanced DNP NMR enables detection of proteins at endogenous levels

- DNP NMR allows specific detection of a protein in complex physiological environments

- Cellular environments alter the structure of intrinsically disordered regions

Authors

Kendra K. Frederick, Vladimir K. Michaelis, Björn Corzilius, Ta-Chung Ong, Angela C. Jacavone, Robert G. Griffin, Susan Lindquist

Correspondence

kendra.frederick@utsouthwestern.edu (K.K.F.),
lindquist_admin@wi.mit.edu (S.L.)

In Brief

Sensitivity-enhanced NMR enabling structural analysis of protein at endogenous levels in a native biological context reveals that the cellular environment alters the structure of an intrinsically disordered protein domain.

CellPress

Article

Cell

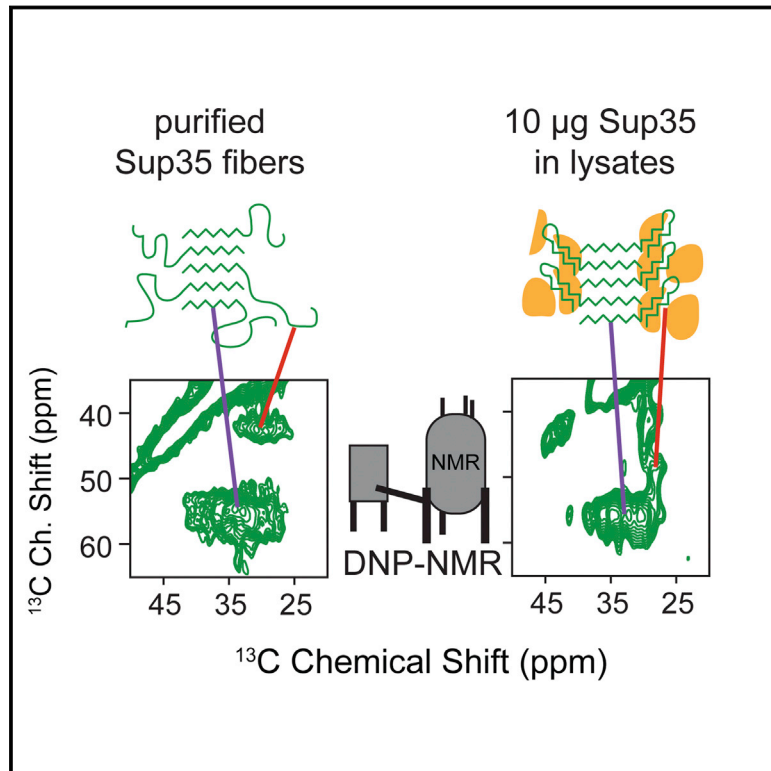# Sensitivity-Enhanced NMR Reveals Alterations in Protein Structure by Cellular Milieus

Kendra K. Frederick,[1,5,*] Vladimir K. Michaelis,[2] Björn Corzilius,[2,6] Ta-Chung Ong,[2,7] Angela C. Jacavone,[2] Robert G. Griffin,[2,4] and Susan Lindquist[1,3,4,*]

[1]Whitehead Institute for Biomedical Research, Cambridge, MA 02142, USA
[2]Department of Chemistry and Francis Bitter Magnet Laboratory, Massachusetts Institute of Technology, Cambridge, MA 02139, USA
[3]Howard Hughes Medical Institute and Department of Biology, Massachusetts Institute of Technology, Cambridge, MA 02139, USA
[4]Co-senior author
[5]Present address: Department of Biophysics, UT Southwestern, Dallas, TX 75390, USA
[6]Present address: Institute of Physical and Theoretical Chemistry, Institute of Biophysical Chemistry, and Center for Biomolecular Magnetic Resonance, Goethe-University, Frankfurt am Main, Germany
[7]Present address: Department of Chemistry, Laboratory of Inorganic Chemistry, ETH-Zürich, CH-8093 Zürich, Switzerland
*Correspondence: kendra.frederick@utsouthwestern.edu (K.K.F.), lindquist_admin@wi.mit.edu (S.L.)
http://dx.doi.org/10.1016/j.cell.2015.09.024

SUMMARY

Biological processes occur in complex environments containing a myriad of potential interactors. Unfortunately, limitations on the sensitivity of biophysical techniques normally restrict structural investigations to purified systems, at concentrations that are orders of magnitude above endogenous levels. Dynamic nuclear polarization (DNP) can dramatically enhance the sensitivity of nuclear magnetic resonance (NMR) spectroscopy and enable structural studies in biologically complex environments. Here, we applied DNP NMR to investigate the structure of a protein containing both an environmentally sensitive folding pathway and an intrinsically disordered region, the yeast prion protein Sup35. We added an exogenously prepared isotopically labeled protein to deuterated lysates, rendering the biological environment "invisible" and enabling highly efficient polarization transfer for DNP. In this environment, structural changes occurred in a region known to influence biological activity but intrinsically disordered in purified samples. Thus, DNP makes structural studies of proteins at endogenous levels in biological contexts possible, and such contexts can influence protein structure.

INTRODUCTION

Structural investigations of biomolecules are typically confined to in vitro systems under limited conditions. Although investigations yield invaluable insights, such experiments can never capture all aspects of complex biological environments. Proteins must fold into their active conformations in complex environments. This situation becomes perilous when considering proteins that must attain a particular conformation, but whose energetic folding landscapes are rather flat or have several local

minima. In these cases, the environment can clearly influence the conformation by favoring one pathway over another. Such decisions can have striking biological consequences, as is the case for a variety of protein folding diseases (Dobson, 2001). The effect of environment becomes even more critical when considering the substantial fraction of the human proteome that encodes disordered proteins (Dunker et al., 2001). Intrinsically disordered proteins (IDPs) are important components of the cellular signaling machinery, allowing the same polypeptide to undertake different interactions with different consequences (Wright and Dyson, 2015). Yet, structural characterization of these domains is notoriously difficult (Uversky, 2013).

Yeast prions present both of these structural challenges as they have both environmentally sensitive protein folding landscapes as well as intrinsically disordered regions. Yeast prions have provided a paradigm shift in our understanding of heritable biological information. They allow specific biological traits to be encoded and inherited solely though self-templating protein conformations. When a protein switches to its prion conformation, its function changes. This altered function is passed from generation to generation by conformational self-templating and catalyzed division of the template to daughter cells. The most extensively studied yeast prion, [PSI+] (Cox, 1965), is an amyloid conformer of the translation termination factor Sup35. In purified amyloid fibrils of the prion domain of Sup35, called NM, the N-terminal domain (N) adopts a beta-sheet-rich amyloid conformation while the adjacent middle domain (M) is intrinsically disordered (Frederick et al., 2014; Krishnan and Lindquist, 2005; Luckgei et al., 2013; Toyama et al., 2007). However, this is unlikely to be the case in vivo: the M domain is known to interact with many other biomolecules, including protein remodeling factors that regulate prion inheritance. As a consequence, mutations in the M domain (Helsen and Glover, 2012; Liu et al., 2002), or changes in the levels of protein chaperones (e.g., Hsp70) and protein remodeling factors (e.g., Hsp104) (Kiktev et al., 2012; Masison et al., 2009; Tuite et al., 2011) have profound effects on prion propagation. NM also physically associates with protein chaperones (Allen et al., 2005), and at least one chaperone binding site has been localized to the M domain of NM (Helsen and Glover, 2012). Finally, a host of genetic data

Cell

suggests that protein-based inheritance is sensitive to the combination and stoichiometry of many other proteins, meaning that isolated study of prion structure can offer at best only partial insight into this paradigm shifting biology.

Interest in prions is highlighted by the fact that similar structural transitions figure in the pathologies of a wide variety of human diseases. Prion strains were first described for the mammalian prion protein, PrP (Chien et al., 2004; Prusiner et al., 1998) and polymorphic amyloid forms have been reported for a variety of amyloidogenic protein associated with neurodegenerative disease (Guo et al., 2013; Kodali et al., 2010; Nekooki-Machida et al., 2009; Petkova et al., 2005). Upon structural characterization, only a portion of the protein is sequestered into the amyloid core. The amyloid cores of these fibers are flanked by intrinsically disordered regions (Heise et al., 2005; Helmus et al., 2008; Wasmer et al., 2009). More recently, amyloid forms of such proteins were demonstrated to have prion-like self-templating dispersion properties in vivo (Jucker and Walker, 2013; Polymenidou and Cleveland, 2012; Watts et al., 2013).

Nuclear magnetic resonance (NMR) is a powerful spectroscopic method for studying molecular structure and dynamics. A key strength of this technique is that it can be used to study non-crystalline, amorphous samples. Indeed, there have been a handful of high-profile in-cell NMR studies (Banci et al., 2013; Freedberg and Selenko, 2014; Inomata et al., 2009; Reckel et al., 2012; Sakakibara et al., 2009; Selenko et al., 2006; Vaiphei et al., 2011). These studies suggest that while protein structure can be perturbed, it is largely unchanged by the cellular context. However, these studies employed solution-state NMR to detect proteins at concentrations two or more orders of magnitude above endogenous levels inside cells, radically altering endogenous stoichiometries. Because solution-state NMR is limited by molecular tumbling times (that depend upon molecular size and solvent viscosity), the minority of the protein that might interact with cellular components would likely be undetectable. Moreover, because this population would comprise a small fraction of the total biomolecule, it would be difficult, if not impossible, to detect the resulting signal loss. Solid state NMR is not limited by molecular correlation times in this way. Instead, solid-state NMR is limited by its low sensitivity. Dynamic nuclear polarization (DNP) has the potential to alleviate this limitation by dramatically increasing the sensitivity of NMR spectroscopy, through the transfer of the large spin polarization that is associated with unpaired electrons to nearby nuclei (Abragam, 1983; Slichter, 1990). Theoretically, DNP can reduce experimental times by more than five orders of magnitude; an experiment that would require decades without DNP can be collected in a day with DNP. However, just as for other structural biology techniques, DNP sensitivity enhancements are critically dependent on experimental conditions (Ni et al., 2013) and sample composition (Akbey et al., 2010, 2013; Takahashi et al., 2014) and the specificity of NMR is critically dependent upon the choice of isotopic labeling (Wang et al., 2013). There is growing interest in application of DNP to complex systems. Several groups have applied DNP to investigate membrane proteins that were over-expressed to high levels in bacteria and have directly examined both concentrated membrane fractions and whole cells (Jacso et al., 2012; Renault et al., 2012; Yamamoto et al., 2015). We

report conditions that enable high polarization transfer efficiencies in biologically complex environments. These are large enough to allow the characterization of a single protein at endogenous concentrations in its native environment. Structural methods to investigate either intrinsically disordered proteins or environmentally sensitive protein folding are limited. Here, we present a generalizable approach for investigation of both of these challenging structural puzzles that lie at the heart of both fundamental biological questions and human diseases. Moreover, we demonstrate that including the biological context can influence protein structure.

RESULTS

NM Adopts an Amyloid Form in Cell Lysates at Low Concentrations

We first confirmed the NM protein adopted its active conformation at endogenous concentrations in a native environment. Previous studies have employed extensive serial dilution and propagation in purified in vitro conditions (Frederick et al., 2014). To ensure that the exogenously added protein was faithfully templated by the prion conformers from the cell lysate, we probed its structural state using semi-denaturing detergent agarose gel electrophoresis (SDD-AGE) (Bagriantsev et al., 2006; Halfmann and Lindquist, 2008). NM did not form amyloid in lysates from cells that do not harbor the [PSI^+] prion form of Sup35 (Figure 1B). In contrast, NM was templated into an amyloid form by both purified pre-formed fibers and lysates from cells that harbored the prion. We determined the concentration of templated, exogenously added NM was ~1 μM by immunoblot (Figure 1C), in good agreement with previously reported endogenous Sup35 concentrations of 2.5–5 μM (Ghaemmaghami et al., 2003). In this way, we prepared samples of isotopically labeled NM amyloids at endogenous levels in a complex biological environment.

Sensitivity and Specificity of DNP Magic Angle Spinning NMR

Having established that NM adopts an amyloid conformation in cellular lysates, we prepared recombinant, ^{1}H, ^{13}C-labeled NM and added it to cell lysates that had been grown in deuterated media with carbon isotopes in natural abundance. This created a spectroscopically active prion protein in an NMR silent cellular background. We prepared the sample for DNP magic angle spinning (MAS) NMR by addition of cryoprotectant (glycerol) and a stable biradical TOTAPOL (Song et al., 2006). We collected 1D ^{13}C{^{1}H} cross polarization (CP) spectra of the cellular lysates both with and without microwave-driven polarization transfer from electrons to nuclei (DNP). Experiments using DNP resulted in significant signal enhancements relative to conventional NMR. DNP signal enhancements (ε) at 211 MHz were between 50- and 115-fold (Figures 2 and S1). The carbonyl carbon enhancements were similar to the maximal enhancements obtained for the reference system proline (ε = 130) for this instrumental configuration. This establishes that DNP MAS NMR is well-suited to study complex biological mixtures.

DNP enhances the NMR signal of all ^{13}C atoms in the sample. Interestingly, in samples with the uniformly ^{13}C-labeled protein at
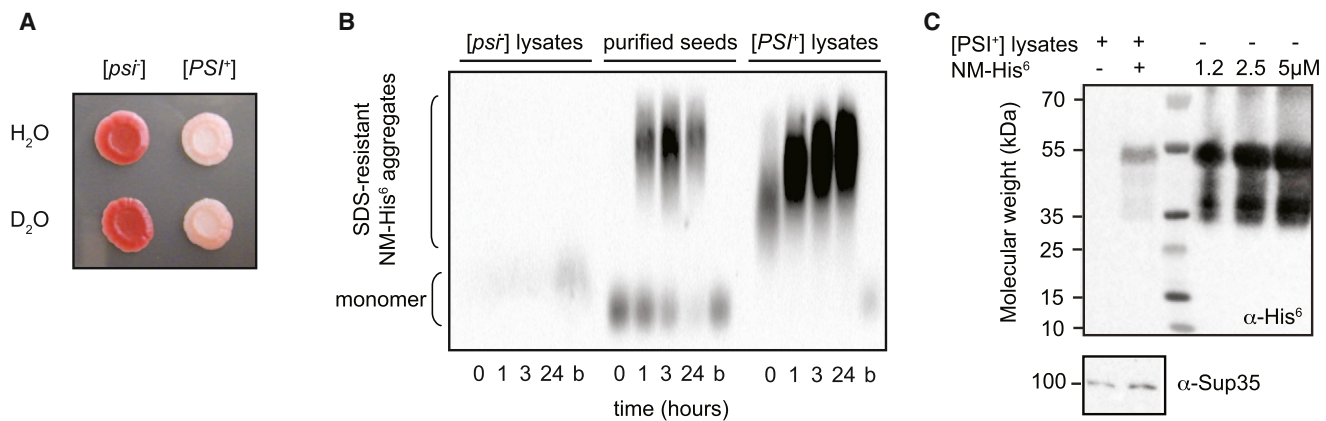
Figure 1. NM Adopts an Amyloid Form in Cell Lysates at Low Concentrations

(A) Prion status is maintained for yeast grown on deuterated media, indicating that the [*PSI*+] protein folding phenotypes were robust to growth in a deuterated environment. Phenotypically prion minus [*psi*−] (red) or prion plus [*PSI*+] (pink) yeasts were grown to mid-log phase in media made with either H_2O or D_2O and then spotted onto a one-fourth YPD plate. Plates were incubated at 30°C for 1 week.

(B) Amyloid formation of purified NM-His[6] was visualized by SDD-AGE using an anti-His[6] antibody in prion minus ([*psi*−]) cell lysates that do not contain endogenous prion templates, in the presence of 2% (w/w) purified amyloid seeds and in prion containing ([*PSI*+]) cellular lysates that contain endogenous prion templates. As with the endogenous prion, boiling (b) destroyed the templated amyloid aggregates.

(C) NM templated into the amyloid form in yeast cell lysates is not degraded and is present at endogenous levels. Full-length endogenous Sup35 runs at 100 kDa and is visualized with an antibody specific to the C-terminal domain. Cellular lysates both with and without exogenously added NM-His[6] as well as a concentration gradient of purified NM-His[6] were boiled in 2% SDS to denature any higher order aggregates and separated by SDS-PAGE before western blotting with an antibody specific for the His[6] epitope. NM-His[6] runs at 55 kDa. The endogenous concentration of Sup35 is between 2.5 and 5 μM. The ECL signal for NM-His[6] in lysates is less intense than that of purified NM-His[6] at a concentration of 1.2 μM, indicating that the concentration of exogenously added NM in the NMR sample is below 1.2 μM.

endogenous concentrations, the ^{13}C content from its natural abundance is an order of magnitude larger than that of added NM protein. However, because the natural abundance of ^{13}C is 1.1%, only 0.01% of the ^{13}C sites in the cell lysate were adjacent to another ^{13}C site. Conversely, all the ^{13}C sites in the exogenously added uniformly ^{13}C-labeled NM had adjacent ^{13}C sites. To isolate ^{13}C signals from NM and filter out background ^{13}C signals from the cell lysates, we collected one-bond [13]C-^{13}C dipolar recoupled correlation spectra using proton driven spin diffusion (PDSD) (Szeverenyi et al., 1982). In this 2D experiment, on-diagonal peaks report on all ^{13}C sites in the sample while off-diagonal peaks, or cross-peaks, report only on ^{13}C sites that are directly bonded to another ^{13}C site. To determine the contributions of cell lysates to the [13]C-^{13}C correlation spectra, we used signals from β1,3-glucan, a major cell wall component that is well-resolved from protein signals. As expected, the ratio of the cross-peak C_1-C_2 signal intensity relative to the diagonal C_1 signal for β1,3-glucan was 2.5% ± 2% of that for yeast grown on uniformly ^{13}C-enriched glucose. However, the ratio of the protein carbonyl carbon (C′)–carbon alpha (C_α) cross-peak signal intensity relative to the diagonal C′ signal intensity for the protein backbone region was 10-fold higher (21% ± 2%) for the natural abundance sample containing added ^{13}C NM than the ratio for the β1,3-glucan region. The protein signal was an order of magnitude larger than the lysate background expected from natural abundance, establishing that the cross-peak signals in the [13]C-^{13}C correlation spectra report on the added NM and not on ^{13}C in the cellular lysates. To completely eliminate any concerns about the contribution of natural abundance ^{13}C from the cellular lysates, samples of prion-containing yeasts for struc-

tural investigations were grown with ^{13}C-depleted (99.9% [12]C) glucose as the carbon source, further reducing the ^{13}C cross-peak intensity from the cellular lysates by two orders of magnitude. Thus, the combination of DNP with this isotopic labeling scheme provides the sensitivity and specificity to observe a protein at endogenous levels in a biologically complex native environment.

To investigate the structural influence of cellular lysates on NM amyloid assembly, we compared spectra of NM fibers at endogenous levels in cellular lysates to spectra of purified lysate-templated NM fibers (Frederick et al., 2014). We conducted these experiments at higher magnetic fields (700 MHz rather than 211 MHz) to achieve significant improvements in spectral resolution (Barnes et al., 2012; Michaelis et al., 2014). We collected a one-bond [13]C-^{13}C dipolar-assisted rotational resonance (DARR) (Takegoshi et al., 2001) correlation spectrum on 1 mg of cryoprotected, purified NM fibrils in 6 hr. For 10 μg of NM fibrils in unlabeled cellular lysates, we collected a one-bond [13]C-^{13}C DARR spectrum for 1 week. As expected, no cross-peaks for β1,3 glucan were present in spectra of cellular lysates grown in depleted ^{13}C glucose. Inhomogeneous line broadening due to experimental temperatures required for DNP (83 K) potentially counteracts any gain in spectral resolution from higher magnetic fields. Thus, we compared spectra of purified NM fibers under DNP conditions to spectra of purified NM fibers at room temperature. In both samples, most of the resonances overlapped due to the number of sites and highly degenerate amino acid composition of this protein, a common feature of prion proteins (Frederick et al., 2014). Nonetheless, the line widths of isolated side chain sites in the DNP spectra at 83 K are similar to those of
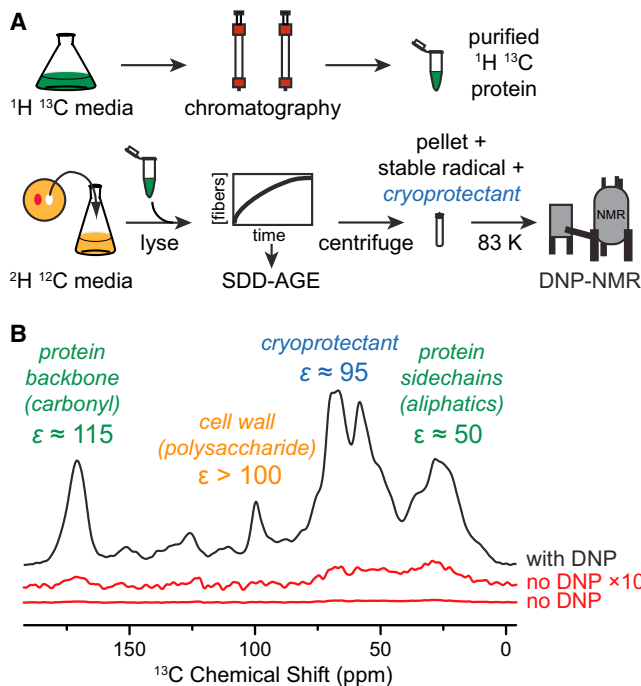
Cell

Figure 2. Dynamic Nuclear Polarization Enhances NMR Signals in Cellular Lysates

(A) Preparation of samples for DNP MAS NMR of proteins at endogenous levels in biological environments. The protein of interest is expressed on isotopically enriched media and purified. The cellular background comes from cells grown on media containing D_2O. The cells are lysed and the isotopically labeled protein is added exogenously to whole lysate. The mixture is pelleted, the pellet is resuspended in a matrix containing stable radical and cryoprotectant, and the mixture is frozen for analysis by DNP MAS NMR.

(B) One-dimensional $^{13}C\{^1H\}$ spectra both with (black) and without DNP enhancement by microwaves (red). Dynamic nuclear polarization gave large signal enhancements (ε) for uniformly ^1H ^{13}C-labeled NM in a deuterated matrix of cellular lysates containing a 60:30:10 (v/v) mixture of d_8-glycerol:D_2O:H_2O and 10 mM TOTAPOL at 211 MHz/140 GHz with $\omega/2\pi = 4.3$ kHz and a sample temperature of 83 K.

See also Figure S1.

room temperature spectra (Figure S2). This establishes that DNP conditions did not compromise resolution gains at high magnetic fields, consistent with several other recent reports for cryogenic experiments on amyloid proteins (Debelouchina et al., 2010; Linden et al., 2011; Lopez del Amo et al., 2013)

Native Environments Structure Intrinsically Disordered Regions

Thus poised, we sought to determine the structural influences of the biological context on NM. The NMR chemical shift is a sensitive indicator of the secondary structure of the protein backbone. To investigate effects of lysates on NM secondary structure, we compared the backbone chemical shifts in the presence and absence of cellular lysates. To isolate signals from backbone C'-C_α sites, we projected the C_α region of the one-bond ^{13}C-^{13}C DARR correlation spectra into one dimension (Figure 3). We fit the carbonyl region of the projections to a sum of three Gaussians that described the chemical shift distributions
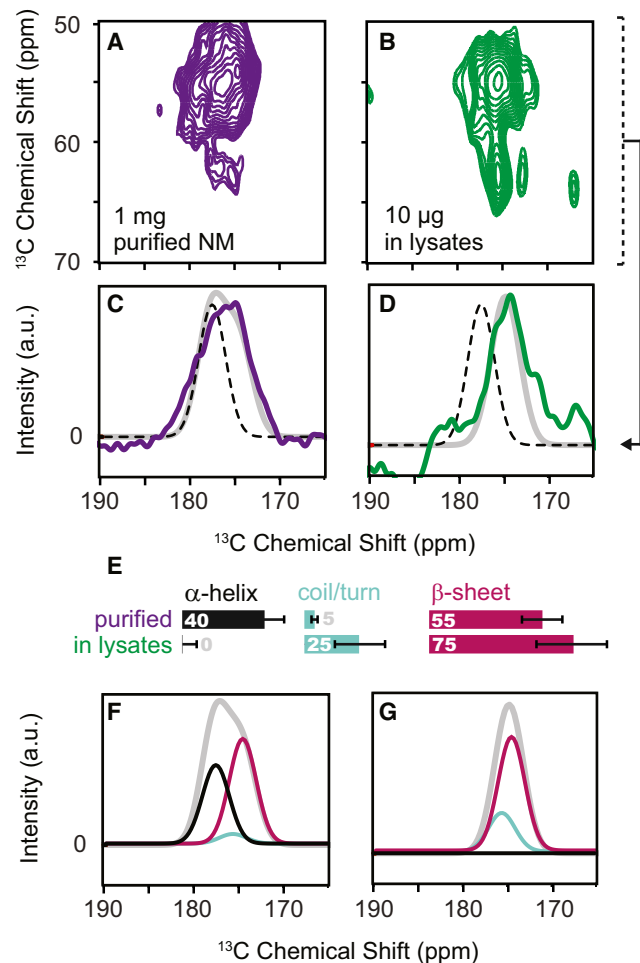

Figure 3. The Secondary Structure of NM Fibers in Cellular Lysates Differs from the Secondary Structure of In Vitro Templated NM

(A and B) Carbonyl carbon region of ^{13}C-^{13}C correlation spectra at 700 MHz using DNP MAS NMR of (A) cryoprotected purified NM fibers acquired in 6 hr and (B) cryoprotected NM fibers assembled in the presence of cellular lysates acquired in 1 week.

(C and D) Examination of the carbonyl carbon (C') region of the spectra in projections of the C_α region (50–70 ppm indicated by dotted bracket) reveals the secondary structural composition of the protein backbone. The projection eliminates signals from non-backbone sites, such as the carbonyl moieties in the amino acid side chains like Asn and Gln. Dotted black lines indicate the expected chemical shift values for α-helical conformations of the protein backbone and highlight a large shift away from α-helical character for NM in lysates (D). The gray line represents the best-fitted solution to three Gaussian distributions describing the expected chemical shifts for the three possible secondary structural motifs: α helices (177.8 $\pm$ 1.5 ppm), random coils and turns (175.6 $\pm$ 1.5 ppm) and beta sheets (175.4 $\pm$ 1.55 ppm) (Wang and Jardetzky, 2002). Fits to a sum of these three Gaussian distributions gave standard estimates of error of 0.84 (C) and 0.93 (D). Residuals are plotted in Figure S3.

(E) Relative secondary structure contributions (in percent) as determined by intensity of each Gaussian distribution for the protein backbone of purified NM fibers (top) and NM fibers assembled in lysates (bottom). The error bars represent the standard error for the fitted intensity of each of the Gaussian distribution.

(F and G) The fitted intensities for α helices (black), random coils and turns (light blue) and beta sheets (magenta) are plotted with the fits (gray) from (C) and (D).

D

MSDSNQGNNQ QNYQQYSQNG NQQQGNNRYQ GYQAYNAQAQ
PAGGYYQNYQ GYSGYQQGGY QQYNPDAGYQ QQYNPQGGYQ
QYNPQGGYQQ QFNPQGGRGN YKNFNYNNNL QGYQAGFQPQ
SQGMSLNDFQ KQQKQAAPKP KKTLKLVSSS GIKLANATKK
VGTKPAESDK KEEEKSAETK EPTKEPTKVE EPVKKEEKPV
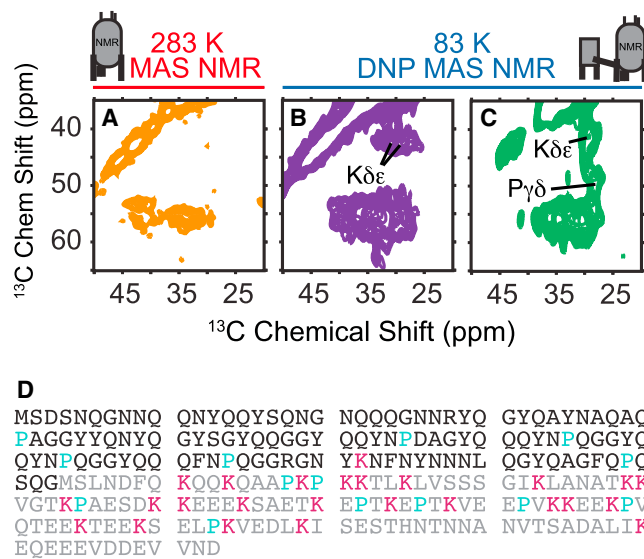QTEEKTEEKS ELPKVEDLKI SESTHNTNNA NVTSADALIK
EQEEEVDDEV VND

Figure 4. Complex Biological Environments Restructure Intrinsically Disordered Protein Regions

(A–C) Side chains of NM fibers in cellular lysates have a different chemical environment than in vitro templated NM. Aliphatic region of (A) purified NM fibers at 283 K in protonated assembly buffer (B) purified NM fibers at 83 K in 60% d_8-glycerol and (C) NM fibers at 83 K in 60% d_8-glycerol templated into the amyloid form in the presence of cellular lysates. See also Figures S2 and S4.

(D) Amino acid sequence of NM with positions of lysines (magenta) and proline (cyan) highlighted. The N domain is black and the M domain is gray.

for α helices, random coil, and beta sheet conformations (Wang and Jardetzky, 2002) (Figure 3). At 283 K, NM fibers experience motion over a broad range of timescales (Frederick et al., 2014). The rigid regions of NM fibers at 283 K had a chemical shift distribution consistent with a mix of turns and sheets (Figure S3). Cryoprotected NM fibers at 83 K had a chemical shift distribution that was dramatically shifted toward α-helical values, consistent with sequence-based secondary structural predictions for the M domain (Chou and Fasman, 1974; Cuff et al., 1998; Kumar, 2013). This change is likely a result of secondary structural stabilization effects from the low experimental temperature and the cryoprotectant (Mehrnejad et al., 2011; Vagenende et al., 2009). In contrast, cryoprotected NM fibers that had been polymerized in cellular lysates had a chemical shift distribution that was dramatically shifted away from α-helical values and toward beta sheet values (Figure 3). Thus, the cellular context had a profound effect on protein secondary structure.

The NMR chemical shift is a sensitive indicator of chemical identity and structural conformation (Wang and Jardetzky, 2002). To determine which amino acid types undergo changes in their secondary structure in cellular contexts, we therefore compared the aliphatic region of the ^{13}C-^{13}C correlation spectra because this region reports on the chemically diverse amino acid side chains. The amyloid core of NM is largely composed of N, Q, and Y residues. In purified room temperature samples, the ^{13}C-^{13}C correlation spectra was consistent with an amyloid core containing N, Q, and Y residues in rigid beta sheet and turn conformations. Changes in the secondary structure at the

α carbon for N, Q, and Y from a beta sheet or random coil conformation to an α-helical conformation result in an average change in chemical shift of ∼4 ppm (Wang and Jardetzky, 2002). The average chemical shift values for this region of the spectra at 83 K for both purified NM and NM in cell lysates were the same as those for the room temperature sample, consistent with the amyloid character of NM being maintained at low temperatures and unperturbed by a biological context (Figures 4 and Figure S4). Thus, the secondary structural changes (Figure 3) were not derived from a structural rearrangement of the amyloid core.

We next compared the aliphatic region of the ^{13}C-^{13}C correlation spectra to determine if amino acid types found in the M domain of NM were affected the biological contexts. In purified room temperature spectra of NM, the ^{13}C-^{13}C correlation spectra was consistent with previous findings that established that the M domain is highly dynamic with random coil character (Frederick et al., 2014; Luckgei et al., 2013); side chain resonances for the amino acid types found only in the M domain were absent. At 83 K, cross-peaks for methyl-bearing amino acids such as threonine, valine, isoleucine and leucine found in the M domain were absent from both spectra due to temperature-dependent dynamically mediated relaxation of methyl-bearing amino acid side chains at this temperature (Bajaj et al., 2009; Beshah et al., 1987). However, at 83 K, lysine Cδ-Cε and proline Cγ-Cδ cross-peaks were present in the DNP MAS NMR spectra of both purified NM and of NM in cell lysates. Unlike the amyloid core residues, these amino acid types had very different chemical environments with differences in chemical shift of 5 ppm or greater depending on whether or not the fibers were templated in cellular lysates (Figure 4). Proline residues are present throughout the sequence of NM, while lysine residues are found only in the M domain (Figure 4D) localizing the regions experiencing large structural changes to the M domain. There are 25 lysine residues in the M domain of NM that contribute to the signal, all of which have different chemical environments and therefore different chemical shifts. The dramatic change in the shape of the lysine Cδ-Cε cross-peak indicates that a large proportion of the lysine side chains have a dramatically altered chemical environment in cellular lysates, indicating the majority of the M domain is involved. This establishes that the M domain, which contains chaperone-binding sites critical for faithful prion inheritance, makes many interactions with such components in vivo.

Multiple lines of evidence reveal that chaperone proteins directly interact with NM fibers. For example, the Hsp70 chaperone proteins Ssa1p and Ssa2p interact with NM aggregates (Allen et al., 2005), are among the top one hundred most highly expressed proteins (Ghaemmaghami et al., 2003) and the major components of amyloid aggregates isolated from yeast (Bagriantsev et al., 2008). In prion-containing cells, NM forms membrane-free cellular structures with specific cellular localizations (Tyedmers et al., 2010). Within these structures, NM amyloid fibers are deposited in highly ordered arrays of regularly spaced fibrils. These arrays consist of bundles of fibers organized by inter-fibrils structures that are thought to be an Hsp70 because cells lacking Hsp70 can no longer form ordered arrays (Saibil et al., 2012). This organization may be important for the faithful

inheritance of the prion by daughter cells or for mitigating the toxicity that is otherwise associated with protein aggregation. The direct observation of NM structure in its biological context indicates that these organizing protein-protein interactions are mediated through the M domain of the protein via the adoption of a beta sheet secondary structure by the majority of this otherwise intrinsically disordered region. This work suggests that disordered regions that are often observed in purified fibril samples may be intimately involved with cellular components to create a self-organization mechanism that coordinates fiber deposition.

DISCUSSION

Application of high-field DNP MAS NMR methodology to a challenging biological system allowed us to pursue a scientific question that was previously impossible due to limits in instrumental sensitivity. Without DNP, these experiments would not be possible. With DNP MAS NMR, we detected prion fibrils that had been assembled in a complex cellular environment containing all of the potential organizing protein components, such as chaperones, at their endogenous levels and stoichiometries. We established such fibers are structurally distinct from purified fibers in a region that is intrinsically disordered and highly dynamic in purified systems. The cellular environment structures an intrinsically disordered region. Sup35 is not unique; over a third of encoded proteins are predicted to be intrinsically disordered (Dunker et al., 2001). Indeed, intrinsically disordered protein regions have important roles in many biological processes, yet their structural characterization is notoriously difficult. Using DNP NMR, we can directly observe a protein of interest in its biological context. We found that the intrinsically disordered domain makes many direct interactions with cellular components. For NM, this suggests the M domain may be responsible for mediating interactions with the inter-fiber structures involved in prion fibril bundle organization visualized using in vivo cryotomography (Saibil et al., 2012).

Our results demonstrate not only that structural studies of proteins in their native contexts are possible, but also that the native context can and does have a dramatic influence on protein structure. We anticipate that our methodology will enable structural investigations of heterotypic quaternary interactions between a protein of interest and cellular constituents. The methods described in this work can be extended to further investigations of protein conformation in biologically relevant environments. For example, protein structures can be determined in cellular contexts that have been modified, either genetically by deletion or overexpression of a protein or by the addition of small molecule agonists. Moreover, because the protein of interest is prepared exogenously, the full suite of specific isotopic enrichment schemes can be employed (Jaipuria et al., 2012) or segmentally isotopically labeled proteins can be used to obtain atomic level structural insights for otherwise crowded spectra (Volkmann and Iwaï, 2010). These approaches will be particularly useful for structural investigations of protein folding and mis-folding in native and perturbed environments. There are a large number of protein folding diseases and work across many fields of study is continually uncovering genetic, physical and chemical modu-

lators of their pathobiology. Our approach will allow direct observation of the structural consequence of such modulators. Thus, this work provides the framework to answer structural questions about the toxic and non-toxic conformations of disease-associated proteins in a way that is directly informed by genetic backgrounds and biological phenotypes. This will allow us to investigate how genetic backgrounds modify the energetic landscape of protein folding and will enable tight coupling of genotypes, phenotypes, and environments with specific structural arrangements.

EXPERIMENTAL PROCEDURES

Sample Preparation

Both untagged NM and C-terminally His[6] tagged NM were expressed and purified as described elsewhere (Serio et al., 1999). Uniformly labeled ^{13}C NM samples were prepared by growing BL21(DES)-Rosetta *Escherichia coli* in the presence of M9 media with 2 g L^{-1} D-glucose ^{1}H,^{13}C$_6$ (Cambridge Isotope Labs). Purified, lysate-templated NM seeds for the purified fiber sample were prepared as described elsewhere (Frederick et al., 2014), using cell lysates from a strong [*PSI*+] yeast strain. One milligram of purified denatured ^{13}C-labeled NM was diluted 120-fold out of 6 M GdHCL into 4 ml of lysis buffer (see below) containing 0.02 mg preformed fibers. The reaction was allowed to polymerize for 24 hr at 4°C and fibers were collected by ultracentrifugation at 430,000 × *g* for 1 hr. Bradford analysis revealed that removal of the supernatant decreased the total protein content of the sample by one-third. The pellet was resuspended in 60:30:10 (v/v/v) mixture of ^{13}C-depleted d_8-glycerol (99.9% ^{12}C):D$_2$O:H$_2$O (Rosay et al., 2010) containing 10 mM of the stable biradical TOTAPOL (Corzilius et al., 2014; Lange et al., 2012; Song et al., 2006).

Cell Lysate Samples for DNP

Phenotypically strong [*PSI*+] yeast were grown in a 20 ml culture volume at 30°C to mid-log phase in YPD media made with protonated carbon sources and 100% D$_2$O. Because we use protonated carbon sources, the final deuteration level for the lysates is estimated to be 70% (Leiting et al., 1998). Cells maintained their [*PSI*+] status in deuterated media (Figure 1A). Cells were collected by centrifugation (5 min, 4,000 × *g*) and washed once with water and once with D$_2$O. Pellets were suspended in 200 μl of lysis buffer (50 mM Tris-HCl pH 7.4, 200 mM NaCl, 2 mM TCEP, 5% d_8-^{13}C-depleted glycerol, 1 mM EDTA, 5 μg/ml of aprotinin and leupeptin and 100 μg/ml Roche protease inhibitor cocktail; lysis buffer was 80% [v/v] D$_2$O.) Cells were lysed by bead beating with 500 μm acid washed glass beads for 8 min at 4°C. After bead beating, the bottom of the Eppendorf tube was punctured with a 22G needle and the entire lysate mixture was transferred to a new tube. Purified denatured ^{13}C-labeled NM was diluted 150-fold out of 6 M GdHCl to a final concentration of 5 μM and the mixture was allowed to polymerize, quiescent, at 4°C for 24 hr. Unassembled NM was removed by centrifugation at 20,000 × *g* for 1 hr at 4°C and removal of the supernatant. The ~30 μl pellet was resuspended in 30 μl of 100% d_8-^{13}C-depleted glycerol containing 20 mM TOTAPOL and transferred to a 4 mm sapphire rotor. The final radical concentration was 10 mM (Corzilius et al., 2014) and the glycerol concentration was 60% (Rosay et al., 2010). The cell lysate sample for high field DNP was made analogously, except that yeast cells were grown in SD-CSM media made with D$_2$O and 2% (w/v) protonated ^{13}C-depleted glucose (99.9% ^{12}C, Cambridge Isotope Labs) as the carbon source. Uniform ^{13}C-labeled samples were grown using U-^{13}C glucose (99% Cambridge Isotope Labs) as the carbon source. The final sample volume was 20 μl and the sapphire rotor had a 3.2-mm diameter.

Immunohistochemistry

Cell lysate samples were made as described above, except NM-His[6] was substituted for NM. SDD-AGE was performed as described (Halfmann and Lindquist, 2008), and NM was visualized using an anti-His[6] antibody. Cell lysates were fractionated by SDS-PAGE, transferred to nitrocellulose and probed with both anti-His[6] and anti-Sup35 antibodies. For SDD-AGE analysis we prepared cellular lysates as described above and added 5 μM purified

Cell

denatured NM-His[6] to reactions containing cellular lysates from prion minus ([*psi*−]) cultures, purified NM fibers prepared in isolation (2% seeding w/w), and cellular lysates from prion plus ([*PSI*+]) cultures. For western blot analysis, lysate samples were denatured by incubation at 95°C for 10 min in the presence of 2% SDS before fractionation to denature amyloid aggregates. Secondary antibodies were coupled to horseradish peroxidase. Blots were visualized by a standard ECL analysis.

Spectroscopy

DNP MAS NMR experiments were performed on custom-designed home-built instruments, consisting of a 212 MHz (^{1}H, 5 T) (Becerra et al., 1993) and a 697 MHz (^{1}H, 16.4 T) (Barnes et al., 2012; Michaelis et al., 2014) NMR spectrometer (courtesy of Dr. David Ruben, Francis Bitter Magnet Laboratory, MIT) equipped with custom-built 140 and 460 GHz gyrotrons (Joye et al., 2006) (i.e., high power microwave devices generating up to 12 W), respectively. DNP MAS NMR spectra were recorded on home-built 4 mm (211 MHz) quadruple resonance (^{1}H, ^{13}C, ^{15}N, and e$^{−}$) or 3.2 mm (700 MHz) triple resonance (^{1}H, ^{13}C, and e$^{−}$) cryogenic probes equipped with Kel-F stators (Revolution NMR). Microwaves were guided to the sample via circular over-moded waveguide in which the inner surface has been corrugated to reduce mode conversion and ohmic losses. Sample temperatures were maintained below 85 K, with spinning frequencies of $\omega_r/2\pi$ = 4.3 – 10 kHz.

^{13}C{^{1}H} cross polarization (Pines et al., 1973) spectra were acquired with a contact time of 1.5 ms. Recycle delays were chosen as T_B (polarization buildup time constant) × 1.26 (Figure S1), yielding optimum sensitivity per unit of time. The recycle delays were 4.6 s and 8 s for 211 MHz and 700 MHz, respectively. A series of ^{13}C-^{13}C DARR spectra were recorded using either a mixing period of 6 or 15 ms, 64–512 co-added transients and, between 60 and 100 t_2 increments. All data were acquired using high-power TPPM ^{1}H decoupling ($\gamma B_1 > 83$ kHz). Enhancements at 211 MHz are reported in Figure 2 and those at 700 MHz were estimated at −8 to −10. DNP enhancements at both fields were ∼80% of the maximal enhancements recorded on a standard sample of proline. Experimental data were processed using RNMR (1D) or NMRpipe (Delaglio et al., 1995) (2D) and analyzed using Sparky (Goddard and Kneller, 2006). ^{13}C NMR data were referenced to adamantane (Morcombe and Zilm, 2003) (40.49 ppm at room temperature), and KBr was used to set the magic angle.

SUPPLEMENTAL INFORMATION

Supplemental Information includes four figures and can be found with this article online at http://dx.doi.org/10.1016/j.cell.2015.09.024.

REFERENCES

Abragam, A. (1983). The Principles of Nuclear Magnetism (Clarendon Press).

Akbey, Ü., Franks, W.T., Linden, A., Lange, S., Griffin, R.G., van Rossum, B.-J., and Oschkinat, H. (2010). Dynamic nuclear polarization of deuterated proteins. Angew. Chem. Int. Ed. Engl. 49, 7803–7806.

Akbey, Ü., Franks, W.T., Linden, A., Orwick-Rydmark, M., Lange, S., and Oschkinat, H. (2013). Dynamic nuclear polarization enhanced NMR in the solid-state. Top. Curr. Chem. 338, 181–228.

Allen, K.D., Wegrzyn, R.D., Chernova, T.A., Müller, S., Newnam, G.P., Winslett, P.A., Wittich, K.B., Wilkinson, K.D., and Chernoff, Y.O. (2005). Hsp70 chaperones as modulators of prion life cycle: novel effects of Ssa and Ssb on the Saccharomyces cerevisiae prion [PSI+]. Genetics 169, 1227–1242.

Bagriantsev, S.N., Kushnirov, V.V., and Liebman, S.W. (2006). Analysis of amyloid aggregates using agarose gel electrophoresis. Methods Enzymol. 412, 33–48.

Bagriantsev, S.N., Gracheva, E.O., Richmond, J.E., and Liebman, S.W. (2008). Variant-specific [PSI+] infection is transmitted by Sup35 polymers within [PSI+] aggregates with heterogeneous protein composition. Mol. Biol. Cell 19, 2433–2443.

Bajaj, V.S., van der Wel, P.C.A., and Griffin, R.G. (2009). Observation of a low-temperature, dynamically driven structural transition in a polypeptide by solid-state NMR spectroscopy. J. Am. Chem. Soc. 131, 118–128.

Banci, L., Barbieri, L., Bertini, I., Luchinat, E., Secci, E., Zhao, Y., and Aricescu, A.R. (2013). Atomic-resolution monitoring of protein maturation in live human cells by NMR. Nat. Chem. Biol. 9, 297–299.

Barnes, A.B., Markhasin, E., Daviso, E., Michaelis, V.K., Nanni, E.A., Jawla, S.K., Mena, E.L., DeRocher, R., Thakkar, A., Woskov, P.P., et al. (2012). Dynamic nuclear polarization at 700 MHz/460 GHz. J. Magn. Reson. 224, 1–7.

Becerra, L.R., Gerfen, G.J., Temkin, R.J., Singel, D.J., and Griffin, R.G. (1993). Dynamic nuclear polarization with a cyclotron resonance mazer at 5 T. Phys. Rev. Lett. 71, 3561–3564.

Beshah, K., Olejniczak, E.T., and Griffin, R.G. (1987). Deuterium NMR study of methyl group dynamics in L-alanine. J. Chem. Phys. 86, 4730.

Chien, P., Weissman, J.S., and DePace, A.H. (2004). Emerging principles of conformation-based prion inheritance. Annu. Rev. Biochem. 73, 617–656.

Chou, P.Y., and Fasman, G.D. (1974). Prediction of protein conformation. Biochemistry 13, 222–245.

Corzilius, B., Andreas, L.B., Smith, A.A., Ni, Q.Z., and Griffin, R.G. (2014). Paramagnet induced signal quenching in MAS-DNP experiments in frozen homogeneous solutions. J. Magn. Reson. 240, 113–123.

Cox, B.S. (1965). Ψ, A cytoplasmic suppressor of super-suppressor in yeast. Heredity 20, 505–521.

Cuff, J.A., Clamp, M.E., Siddiqui, A.S., Finlay, M., and Barton, G.J. (1998). JPred: a consensus secondary structure prediction server. Bioinformatics 14, 892–893.

Debelouchina, G.T., Bayro, M.J., van der Wel, P.C.A., Caporini, M.A., Barnes, A.B., Rosay, M., Maas, W.E., and Griffin, R.G. (2010). Dynamic nuclear polarization-enhanced solid-state NMR spectroscopy of GNNQQNY nanocrystals and amyloid fibrils. Phys. Chem. Chem. Phys. 12, 5911–5919.

Delaglio, F., Grzesiek, S., Vuister, G.W., Zhu, G., Pfeifer, J., and Bax, A. (1995). NMRPipe: a multidimensional spectral processing system based on UNIX pipes. J. Biomol. NMR 6, 277–293.

Dobson, C.M. (2001). The structural basis of protein folding and its links with human disease. Philos. Trans. R. Soc. Lond. B Biol. Sci. 356, 133–145.

Dunker, A.K., Lawson, J.D., Brown, C.J., Williams, R.M., Romero, P., Oh, J.S., Oldfield, C.J., Campen, A.M., Ratliff, C.M., Hipps, K.W., et al. (2001). Intrinsically disordered protein. J. Mol. Graph. Model. 19, 26–59.

Frederick, K.K., Debelouchina, G.T., Kayatekin, C., Dorminy, T., Jacavone, A.C., Griffin, R.G., and Lindquist, S. (2014). Distinct prion strains are defined by amyloid core structure and chaperone binding site dynamics. Chem. Biol. 21, 295–305.

Freedberg, D.I., and Selenko, P. (2014). Live cell NMR. Annu. Rev. Biophys. *43*, 171–192.

Ghaemmaghami, S., Huh, W.-K., Bower, K., Howson, R.W., Belle, A., Dephoure, N., O'Shea, E.K., and Weissman, J.S. (2003). Global analysis of protein expression in yeast. Nature *425*, 737–741.

Goddard, T.D., and Kneller, D.G. (2006). Sparky (University of California).

Guo, J.L., Covell, D.J., Daniels, J.P., Iba, M., Stieber, A., Zhang, B., Riddle, D.M., Kwong, L.K., Xu, Y., Trojanowski, J.Q., and Lee, V.M. (2013). Distinct α-synuclein strains differentially promote tau inclusions in neurons. Cell *154*, 103–117.

Halfmann, R., and Lindquist, S. (2008). Screening for amyloid aggregation by semi-denaturing detergent-agarose gel electrophoresis. J. Vis. Exp. *17*, 838.

Heise, H., Hoyer, W., Becker, S., Andronesi, O.C., Riedel, D., and Baldus, M. (2005). Molecular-level secondary structure, polymorphism, and dynamics of full-length alpha-synuclein fibrils studied by solid-state NMR. Proc. Natl. Acad. Sci. USA *102*, 15871–15876.

Helmus, J.J., Surewicz, K., Nadaud, P.S., Surewicz, W.K., and Jaroniec, C.P. (2008). Molecular conformation and dynamics of the Y145Stop variant of human prion protein in amyloid fibrils. Proc. Natl. Acad. Sci. USA *105*, 6284–6289.

Helsen, C.W., and Glover, J.R. (2012). Insight into molecular basis of curing of [PSI+] prion by overexpression of 104-kDa heat shock protein (Hsp104). J. Biol. Chem. *287*, 542–556.

Inomata, K., Ohno, A., Tochio, H., Isogai, S., Tenno, T., Nakase, I., Takeuchi, T., Futaki, S., Ito, Y., Hiroaki, H., and Shirakawa, M. (2009). High-resolution multi-dimensional NMR spectroscopy of proteins in human cells. Nature *458*, 106–109.

Jacso, T., Franks, W.T., Rose, H., Fink, U., Broecker, J., Keller, S., Oschkinat, H., and Reif, B. (2012). Characterization of membrane proteins in isolated native cellular membranes by dynamic nuclear polarization solid-state NMR spectroscopy without purification and reconstitution. Angew. Chem. Int. Ed. Engl. *51*, 432–435.

Jaipuria, G., Krishnarjuna, B., Mondal, S., Dubey, A., and Atreya, H.S. (2012). Amino acid selective labeling and unlabeling for protein resonance assignments. Adv. Exp. Med. Biol. *992*, 95–118.

Joye, C.D., Griffin, R.G., Hornstein, M.K., Hu, K.-N., Kreischer, K.E., Rosay, M., Shapiro, M.A., Sirigiri, J.R., Temkin, R.J., and Woskov, P.P. (2006). Operational characteristics of a 14-W 140-GHz gyrotron for dynamic nuclear polarization. IEEE Trans Plasma Sci IEEE Nucl Plasma Sci Soc *34*, 518–523.

Jucker, M., and Walker, L.C. (2013). Self-propagation of pathogenic protein aggregates in neurodegenerative diseases. Nature *501*, 45–51.

Kiktev, D.A., Patterson, J.C., Müller, S., Bariar, B., Pan, T., and Chernoff, Y.O. (2012). Regulation of chaperone effects on a yeast prion by cochaperone Sgt2. Mol. Cell. Biol. *32*, 4960–4970.

Kodali, R., Williams, A.D., Chemuru, S., and Wetzel, R. (2010). Aβ(1–40) Forms five distinct amyloid structures whose β-sheet contents and fibril stabilities are correlated. J. Mol. Biol. *401*, 503–517.

Krishnan, R., and Lindquist, S.L. (2005). Structural insights into a yeast prion illuminate nucleation and strain diversity. Nature *435*, 765–772.

Kumar, T.A. (2013). CFSSP: Chou and Fasman Secondary Structure Prediction Server. Wide Spectrum *1*, 15–19.

Lange, S., Linden, A.H., Akbey, Ü., Franks, W.T., Loening, N.M., van Rossum, B.-J., and Oschkinat, H. (2012). The effect of biradical concentration on the performance of DNP-MAS-NMR. J. Magn. Reson. *216*, 209–212.

Leiting, B., Marsilio, F., and O'Connell, J.F. (1998). Predictable deuteration of recombinant proteins expressed in Escherichia coli. Anal. Biochem. *265*, 351–355.

Linden, A.H., Franks, W.T., Akbey, Ü., Lange, S., van Rossum, B.-J., and Oschkinat, H. (2011). Cryogenic temperature effects and resolution upon slow cooling of protein preparations in solid state NMR. J. Biomol. NMR *51*, 283–292.

Liu, J.-J., Sondheimer, N., and Lindquist, S.L. (2002). Changes in the middle region of Sup35 profoundly alter the nature of epigenetic inheritance for the yeast prion [PSI+]. Proc. Natl. Acad. Sci. USA *99* (*Suppl 4*), 16446–16453.

Lopez del Amo, J.-M., Schneider, D., Loquet, A., Lange, A., and Reif, B. (2013). Cryogenic solid state NMR studies of fibrils of the Alzheimer's disease amyloid-β peptide: perspectives for DNP. J. Biomol. NMR *56*, 359–363.

Luckgei, N., Schütz, A.K., Bousset, L., Habenstein, B., Sourigues, Y., Gardiennet, C., Meier, B.H., Melki, R., and Böckmann, A. (2013). The conformation of the prion domain of Sup35p in isolation and in the full-length protein. Angew. Chem. Int. Ed. Engl. *52*, 12741–12744.

Masison, D.C., Kirkland, P.A., and Sharma, D. (2009). Influence of Hsp70s and their regulators on yeast prion propagation. Prion *3*, 65–73.

Mehrnejad, F., Ghahremanpour, M.M., Khadem-Maaref, M., and Doustdar, F. (2011). Effects of osmolytes on the helical conformation of model peptide: molecular dynamics simulation. J. Chem. Phys. *134*, 035104.

Michaelis, V.K., Ong, T.-C., Kiesewetter, M.K., Frantz, D.K., Walish, J.J., Ravera, E., Luchinat, C., Swager, T.M., and Griffin, R.G. (2014). Topical Developments in High-Field Dynamic Nuclear Polarization. Isr. J. Chem. *54*, 207–221.

Morcombe, C.R., and Zilm, K.W. (2003). Chemical shift referencing in MAS solid state NMR. J. Magn. Reson. *162*, 479–486.

Nekooki-Machida, Y., Kurosawa, M., Nukina, N., Ito, K., Oda, T., and Tanaka, M. (2009). Distinct conformations of in vitro and in vivo amyloids of huntingtin-exon1 show different cytotoxicity. Proc. Natl. Acad. Sci. USA *106*, 9679–9684.

Ni, Q.Z., Daviso, E., Can, T.V., Markhasin, E., Jawla, S.K., Swager, T.M., Temkin, R.J., Herzfeld, J., and Griffin, R.G. (2013). High frequency dynamic nuclear polarization. Acc. Chem. Res. *46*, 1933–1941.

Petkova, A.T., Leapman, R.D., Guo, Z., Yau, W.-M., Mattson, M.P., and Tycko, R. (2005). Self-propagating, molecular-level polymorphism in Alzheimer's beta-amyloid fibrils. Science *307*, 262–265.

Pines, A., Gibby, M.G., and Waugh, J.S. (1973). Proton-enhanced NMR of dilute spins in solids. J. Chem. Phys. *59*, 569.

Polymenidou, M., and Cleveland, D.W. (2012). Prion-like spread of protein aggregates in neurodegeneration. J. Exp. Med. *209*, 889–893.

Prusiner, S.B., Scott, M.R., DeArmond, S.J., and Cohen, F.E. (1998). Prion protein biology. Cell *93*, 337–348.

Reckel, S., Lopez, J.J., Löhr, F., Glaubitz, C., and Dötsch, V. (2012). In-cell solid-state NMR as a tool to study proteins in large complexes. ChemBioChem *13*, 534–537.

Renault, M., Pawsey, S., Bos, M.P., Koers, E.J., Nand, D., Tommassen-van Boxtel, R., Rosay, M., Tommassen, J., Maas, W.E., and Baldus, M. (2012). Solid-state NMR spectroscopy on cellular preparations enhanced by dynamic nuclear polarization. Angew. Chem. Int. Ed. Engl. *51*, 2998–3001.

Rosay, M., Tometich, L., Pawsey, S., Bader, R., Schauwecker, R., Blank, M., Borchard, P.M., Cauffman, S.R., Felch, K.L., Weber, R.T., Temkin, R.J., Griffin, R.G., and Maas, W.E. (2010). Solid-state dynamic nuclear polarization at 263 GHz: spectrometer design and experimental results. Phys. Chem. Chem. Phys. *12*, 5850–5860.

Saibil, H.R., Seybert, A., Habermann, A., Winkler, J., Eltsov, M., Perkovic, M., Castaño-Diez, D., Scheffer, M.P., Haselmann, U., Chlanda, P., et al. (2012). Heritable yeast prions have a highly organized three-dimensional architecture with interfiber structures. Proc. Natl. Acad. Sci. USA *109*, 14906–14911.

Sakakibara, D., Sasaki, A., Ikeya, T., Hamatsu, J., Hanashima, T., Mishima, M., Yoshimasu, M., Hayashi, N., Mikawa, T., Wälchli, M., et al. (2009). Protein structure determination in living cells by in-cell NMR spectroscopy. Nature *458*, 102–105.

Selenko, P., Serber, Z., Gadea, B., Ruderman, J., and Wagner, G. (2006). Quantitative NMR analysis of the protein G B1 domain in Xenopus laevis egg extracts and intact oocytes. Proc. Natl. Acad. Sci. USA *103*, 11904–11909.

Serio, T.R., Cashikar, A.G., Moslehi, J.J., Kowal, A.S., and Lindquist, S.L. (1999). Yeast prion [psi +] and its determinant, Sup35p. Methods Enzymol. *309*, 649–673.

Slichter, C.P. (1990). Principles of Magnetic Resonance (Springer Science and Business Media).

Song, C., Hu, K.-N., Joo, C.-G., Swager, T.M., and Griffin, R.G. (2006). TOTA-POL: a biradical polarizing agent for dynamic nuclear polarization experiments in aqueous media. J. Am. Chem. Soc. 128, 11385–11390.

Szeverenyi, N.M., Sullivan, M.J., and Maciel, G.E. (1982). Observation of spin exchange by two-dimensional fourier transform 13C cross polarization-magic-angle spinning. J. Magn. Reson. (1969) 47, 462–475.

Takahashi, H., Fernández-de-Alba, C., Lee, D., Maurel, V., Gambarelli, S., Bardet, M., Hediger, S., Barra, A.-L., and De Paëpe, G. (2014). Optimization of an absolute sensitivity in a glassy matrix during DNP-enhanced multidimensional solid-state NMR experiments. J. Magn. Reson. 239, 91–99.

Takegoshi, K., Nakamura, S., and Terao, T. (2001). ^{13}C-^{1}H dipolar-assisted rotational resonance in magic-angle spinning NMR. Chem. Phys. Lett. 344, 631–637.

Toyama, B.H., Kelly, M.J.S., Gross, J.D., and Weissman, J.S. (2007). The structural basis of yeast prion strain variants. Nature 449, 233–237.

Tuite, M.F., Marchante, R., and Kushnirov, V. (2011). Fungal prions: structure, function and propagation. Top. Curr. Chem. 305, 257–298.

Tyedmers, J., Treusch, S., Dong, J., McCaffery, J.M., Bevis, B., and Lindquist, S. (2010). Prion induction involves an ancient system for the sequestration of aggregated proteins and heritable changes in prion fragmentation. Proc. Natl. Acad. Sci. USA 107, 8633–8638.

Uversky, V.N. (2013). A decade and a half of protein intrinsic disorder: biology still waits for physics. Protein Sci. 22, 693–724.

Vagenende, V., Yap, M.G.S., and Trout, B.L. (2009). Mechanisms of protein stabilization and prevention of protein aggregation by glycerol. Biochemistry 48, 11084–11096.

Vaiphei, S.T., Tang, Y., Montelione, G.T., and Inouye, M. (2011). The use of the condensed single protein production system for isotope-labeled outer membrane proteins, OmpA and OmpX in E. coli. Mol. Biotechnol. 47, 205–210.

Volkmann, G., and Iwaï, H. (2010). Protein trans-splicing and its use in structural biology: opportunities and limitations. Mol. Biosyst. 6, 2110–2121.

Wang, Y., and Jardetzky, O. (2002). Probability-based protein secondary structure identification using combined NMR chemical-shift data. Protein Sci. 11, 852–861.

Wang, T., Park, Y.B., Caporini, M.A., Rosay, M., Zhong, L., Cosgrove, D.J., and Hong, M. (2013). Sensitivity-enhanced solid-state NMR detection of expansin's target in plant cell walls. Proc. Natl. Acad. Sci. USA 110, 16444–16449.

Wasmer, C., Schütz, A., Loquet, A., Buhtz, C., Greenwald, J., Riek, R., Böckmann, A., and Meier, B.H. (2009). The molecular organization of the fungal prion HET-s in its amyloid form. J. Mol. Biol. 394, 119–127.

Watts, J.C., Giles, K., Oehler, A., Middleton, L., Dexter, D.T., Gentleman, S.M., DeArmond, S.J., and Prusiner, S.B. (2013). Transmission of multiple system atrophy prions to transgenic mice. Proc. Natl. Acad. Sci. USA 110, 19555–19560.

Wright, P.E., and Dyson, H.J. (2015). Intrinsically disordered proteins incellular signalling and regulation. Nat. Rev. Mol. Cell Biol. 16, 18–29.

Yamamoto, K., Caporini, M.A., Im, S.-C., Waskell, L., and Ramamoorthy, A. (2015). Cellular solid-state NMR investigation of a membrane protein using dynamic nuclear polarization. Biochim. Biophys. Acta 1848, 342–349.